HHS Public Access

Author manuscript

ACS Nano. Author manuscript; available in PMC 2021 August 25.

Published in final edited form as:

ACS Nano. 2020 August 25; 14(8): 10187–10197. doi:10.1021/acsnano.0c03457.

Dextran Coated Cerium Oxide Nanoparticles: A Computed Tomography Contrast Agent for Imaging the Gastrointestinal Tract and Inflammatory Bowel Disease

Pratap C. Naha[1,*], **Jessica C. Hsu**[1,2], **Johoon Kim**[1,2], **Shrey Shah**[1,2], **Mathilde Bouché**[1], **Salim Si-Mohamed**[3,4], **Derick N. Rosario-Berrios**[5], **Philippe Douek**[3,4], **Maryam Hajfathalian**[1], **Parisa Yasini**[6], **Sanjay Singh**[7], **Mark A. Rosen**[1], **Matthew A. Morgan**[1], **David P. Cormode**[1,2,8,*]

[1]Department of Radiology, University of Pennsylvania, Philadelphia, Pennsylvania, USA, 19104

[2]Bioengineering, University of Pennsylvania, Philadelphia, Pennsylvania, USA, 19104

[3]Department of Radiology, Hôpital Cardio-Vasculaire et Pneumologique Louis Pradel, Lyon, France, 69500

[4]Centre de Recherche en Acquisition et Traitement de l'Image pour la Santé (CREATIS), UMR CNRS 5220, Inserm U1044, University Lyon1 Claude Bernard, Lyon, France, 69621

[5]Biochemistry and Molecular Biophysics, University of Pennsylvania, Philadelphia, Pennsylvania, USA, 19104

[6]Department of Chemistry, Temple University, Philadelphia, Pennsylvania, USA, 19122

[7]Division of Biological and Life Sciences School of Arts and Sciences Ahmedabad University, Ahmedabad, Gujarat, India, 380009

[8]Medicine, Division of Cardiovascular Medicine, University of Pennsylvania, Philadelphia, Pennsylvania, USA, 19104

Abstract

Computed tomography (CT) is an x-ray based medical imaging technique commonly used for non-invasive gastrointestinal tract (GIT) imaging. Iodine and barium based CT contrast agents are used in the clinic for GIT imaging, however, inflammatory bowel disease (IBD) imaging is challenging since iodinated and barium based CT agents are not specific for sites of inflammation. Cerium oxide nanoparticles (CeNP) can produce strong x-ray attenuation due to cerium's k-edge at 40.4 keV, but have not yet been explored for CT imaging. In addition, we hypothesized that the use of dextran as a coating material on cerium oxide nanoparticles would encourage accumulation in IBD inflammation sites in a similar fashion to other inflammatory diseases. In this study, therefore, we sought to develop a CT contrast agent, *i.e.* dextran coated cerium oxide nanoparticles

[*]Corresponding authors: University of Pennsylvania, 3400 Spruce St, 1 Silverstein, Philadelphia, PA 19104, USA, pratap.naha@pennmedicine.upenn.edu and david.cormode@pennmedicine.upenn.edu.

Supplementary information

Micro CT phantom image and analysis, SPCCT phantom images, CT images and analysis for healthy mice, biodistribution data, tables of statistical data. This material is available free of charge *via* the Internet at http://pubs.acs.org.

(Dex-CeNP) for GIT imaging with IBD. We synthesized Dex-CeNP, characterized them using various analytical tools and examined their *in vitro* biocompatibility, CT contrast generation and protective effect against oxidative stress. *In vivo* CT imaging was done with both healthy mice and a dextran sodium sulfate induced colitis (DSS-colitis) mouse model. Dex-CeNP's CT contrast generation and accumulation in inflammation sites were compared with iopamidol, an FDA approved CT contrast agent. Dex-CeNP was found to be protective against oxidative damage. Dex-CeNP produced strong CT contrast and accumulated in the colitis area of large intestines. In addition, >97 % of oral doses were cleared from the body within 24 hrs. Therefore, Dex-CeNP can be used as a potential CT contrast agent for imaging GIT with IBD, while protecting against oxidative damage.

Graphical Abstract

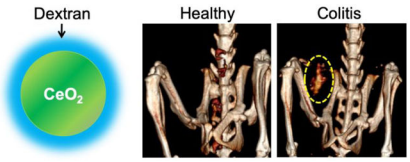

Keywords

cerium oxide; computed tomography; colitis; nanoparticles; contrast agent

Computed tomography (CT), used in conjunction with contrast agents, is invaluable for imaging the cardiovascular system[1–3] and gastrointestinal tract (GIT).[4–8] Iodinated small molecules and barium sulfate suspensions are used in the clinic for GIT imaging.[4–6, 9] However, the image quality of iodine-enhanced CT is poor for imaging the abdomen in overweight and obese patients,[10, 11] and is not ideal for imaging inflammatory bowel disease (IBD) due to its non-specificity. Moreover, iodinated CT agents are found to be extravasated when administered to patients.[12] Therefore, it is expected that small molecule based CT agents, when administered orally, can be absorbed through the GIT and surrounding tissues, thus interfering with diagnosis. In addition, patients with IBD may receive many CT scans over the course of their lives and will therefore accumulate radiation exposure.[13] Therefore, patients with IBD would benefit from an alternative CT contrast agent for GIT imaging that could mitigate the effects of radiation exposure.

Nanoparticles have been the focus of much attention for their use as CT contrast agents,[3] since it is relatively easy to synthesize them with different sizes and coatings, which can provide specificity to different types of disease sites.[14–17] Nanoparticle based CT contrast agents should not diffuse through intact GIT due to their large size compared with the cellular junctions in the walls of these organs, but have potential to accumulate in sites of inflammation, where cellular junctions are disrupted, as found in IBD. Despite the theoretical potential of nanoparticle based CT contrast agents for IBD imaging, there have been no such studies reported to date, to the best of our knowledge. Gold nanoparticles have been proposed as CT contrast agents, since they are inert, non-toxic, easy to synthesize, and

produce strong CT contrast.[1, 18, 19] However, the relatively high cost of gold might be a challenge for their translation into the clinic.

Cerium oxide nanoparticles could be alternative CT contrast agents. Cerium has a k-edge at 40.4 keV, slightly higher than that of iodine (33.2 keV), and well matched to the x-ray beams used in medical imaging,[3] therefore it should produce strong CT contrast. In addition to this, dextran coating on cerium oxide nanoparticle surfaces should provide stability in aqueous media, biocompatibility, and specificity towards inflammation sites.[20, 21] Moreover, cerium oxide nanoparticles have been proposed as an artificial reactive oxygen species (ROS) scavenger, since they can neutralize free radicals.[22–25] X-ray irradiation induces free radical generation in the exposed cells or tissues, which can cause damage.[26, 27] Cerium oxide nanoparticles have been shown to protect cells from radiation induced toxicity[22] as well as animals from several external stress sources.[28–31] They also show strong anti-apoptotic effects,[32, 33] improve many serious oxidation related pathologies[28–30] and promote wound healing.[28] Moreover, cerium is inexpensive and, to the best of our knowledge, has barely been explored as a basis for CT contrast agents.

In this study, we report that dextran coated cerium oxide nanoparticles (Dex-CeNP, Figure 1) can be used as a CT contrast agent for GIT imaging with or without IBD and can protect cells from oxidative damage. Dex-CeNP was synthesized *via* a precipitation method and was characterized *via* several analytical tools. Their CT contrast generation property was investigated with a clinical CT scanner. *In vitro* biocompatibility was tested with four different cell types and their ability to protect cells against oxidative damage was investigated. The *in vivo* properties of Dex-CeNP were investigated with healthy mice and dextran sodium sulfate induced colitis (DSS-induced colitis) mice *via* CT imaging. The biodistribution of Dex-CeNP was studied in healthy and DSS-colitis mice. Localization of Dex-CeNP in the large intestine of DSS-colitis mice was investigated *via* electron microscopy. Last, histopathological analyses on the stomachs, small intestines and large intestines of the mice were used to probe the safety of Dex-CeNP.

Results and Discussion

Synthesis and Characterization

Dex-CeNP was formed *via* precipitation of cerium salts after addition to ammonium hydroxide in the presence of dextran. Dex-CeNP were well suspended in phosphate buffered saline (PBS) and had a UV-visible absorbance peak at 290 nm (Figure 1B and C). The core and hydrodynamic diameter of Dex-CeNP were found to be 4.8 ± 1.2 nm (Figure 1D) and 17.5 ± 0.7 nm respectively. As expected, the hydrodynamic diameter was found to be larger than the core diameter due to the dextran coating. The zeta potential of Dex-CeNP was found to be −8 ± 0.7 mV, which is similar to the surface potential observed for other dextran coated nanoparticles.[20, 34] High resolution transmission electron microscopy (HR-TEM) revealed the crystalline lattice structure of the cerium oxide core (Figure 1D, white boxed area). In addition, the powder x-ray diffraction (XRD) pattern included several characteristic diffraction peaks of cerium oxide nanocrystals (Figure 1E). The cerium oxide cores in Dex-CeNP were found to be face centered cubic (FCC) crystals since the XRD pattern showed the presence of (111), (220), (311), and (331) planes.[35]

FT-IR confirmed the presence of the dextran coating in the purified nanoparticles (Figure 1F). The characteristic peaks of dextran in the spectrum of Dex-CeNP were found to match well with those of free dextran (Figure 1F). Notably, the intense peaks at 3392 cm^{-1}, 2924 cm^{-1}, and 1153 cm^{-1} corresponded to the O-H stretching of the hydroxyl group, the stretching of the C-H bond, and the C-O-C vibration of the glycosidic bridge between saccharide units, respectively.[36, 37]

CT contrast generation properties

The CT contrast generation properties of Dex-CeNP were investigated using a clinical CT scanner (Siemens SOMATOM Force). Iopamidol (an FDA approved CT contrast agent) and gold nanoparticles were used as controls. The phantom was scanned with four different tube voltages, *i.e.* 80, 100, 120 and 140 kV. A representative Dex-CeNP phantom image scanned at 80 kV is presented in Figure 2A. The CT attenuation of Dex-CeNP was found to be linearly correlated with the mass concentration of cerium (r^2= 0.99) for each tube voltage used (Figure 2B). The CT attenuation rates of different agents, *i.e.* Dex-CeNP, cerium nitrate, iopamidol, and gold nanoparticles are presented in Figure 2C.

Dex-CeNP produced greater CT attenuation when scanned at 80 kV compared to 100, 120 or 140 kV and the attenuation values found were similar to those for cerium salt. The CT attenuation rate decreased with increasing tube voltage, which was expected since the average beam energy moves further away from cerium's k-edge, *i.e.* 40.4 keV, as the tube voltage increases. When compared with iopamidol, Dex-CeNP produced a slightly greater CT attenuation rate at each tube voltage used (Figure 2C). This is because iodine has a slightly lower k-edge value (*i.e.* 33.2 keV) than cerium and is therefore always further from the average of the beam energy. However, in the case of gold nanoparticles, the CT attenuation rate was found to increase with increasing tube voltage (Figure 2C), in agreement with previous observations,[16] and was higher than that produced by Dex-CeNP at 140 kV. When scanned with a Molecubes microCT (Figure S1), we found an attenuation rate of 47.9 HU.ml/mg, which is very similar to the attenuation found from the clinical scanner at 80 kV, *i.e.* 44.0 HU.ml/mg. Moreover, we scanned a phantom of Dex-CeNP with a clinical-scale spectral photon counting CT (SPCCT) system and found that specific Dex-CeNP imaging could be done with this system (Figure S2).

In vitro biocompatibility

In vitro biocompatibility of Dex-CeNP was investigated in human hepatocellular liver carcinoma (HepG2), human fibroblast (BJ5ta), human colorectal adenocarcinoma (C2BBe1), and murine macrophage (J774A.1) at 1 and 24 hrs. The 24 hrs timepoint is particularly relevant, since almost all of the agent was cleared by 24 hrs *in vivo* (see later). The effect of Dex-CeNP exposure on the viability of these cells was measured and is presented in Figure 3. No substantial adverse effect was observed for any cell type or condition examined.

Protective effect of Dex-CeNP against oxidative damage

Cerium oxide nanoparticles have been shown to act as artificial ROS scavengers[22, 23, 38] since cerium ions can switch between Ce^{3+} and Ce^{4+} oxidation states.[24, 30, 39, 40] The

Ce^{3+}/Ce^{4+} redox couple has been shown to catalyze the reduction of hydrogen peroxide to form water and oxygen in a catalase-like fashion.[39, 40] A schematic of the oxidation-reduction cycle of cerium oxide nanoparticles is presented in Figure 4A. We explored the protective effect of Dex-CeNP with two different cell types using hydrogen peroxide as an oxidative toxic chemical. We found that hydrogen peroxide alone significantly lowered cell viability. However, when the cells were treated with both Dex-CeNP and hydrogen peroxide, no difference in cell viability was found between control and treatment groups, indicating that Dex-CeNP protected the cells from oxidative damage induced by hydrogen peroxide (Figure 4B and C).

In vivo CT imaging

Due to the promising *in vitro* results, we were motivated to explore the feasibility of imaging IBD using Dex-CeNP as a CT imaging probe. *In vivo* CT imaging with Dex-CeNP or iopamidol was performed with healthy and DSS-induced colitis mice. Representative CT images of healthy mice before and after treatment with Dex-CeNP or iopamidol are presented in Figure S3A. Quantitative analyses of the CT contrast from the stomach, small intestine and large intestine are presented in Figure S3B. Tables of statistical comparisons are included in the supporting information. Strong contrast was observed in different sections of the GIT at different time points. We found that there was no substantial difference in the CT contrast observed for Dex-CeNP compared to iopamidol in healthy mice, indicating the potential of Dex-CeNP for GIT imaging (Figure S3).

On the other hand, a different result was observed for DSS-induced colitis mice that received Dex-CeNP or iopamidol. Representative CT images of DSS-colitis mice before and after treatment with Dex-CeNP or iopamidol and their quantitative analyses are presented in Figure 5A and B, respectively. The change in CT attenuation in the large intestine was found to be significantly greater when colitis mice received Dex-CeNP compared to iopamidol, except at 5 and 30 minutes post-administration (Figure 5B). This may be due to differences in the way that iopamidol (a small molecule) and Dex-CeNP (a nanoparticle) diffuse within the diseased tissue.

When comparing healthy and colitis mice that received Dex-CeNP, higher CT attenuation was observed in the large intestine of colitis mice at 60 and 120 minutes post-administration. Moreover, no CT contrast was observed in the large intestine of the healthy mice at 24 hrs post-administration, but marked attenuation was observed for colitis mice (Figure 6A,B). This finding from microCT should translate to very similar contrast for clinical CT scans performed at 80 kV, since the contrast generation of Dex-CeNP is almost equivalent between the two types of scanner (Figures 2 and S1). We did not find cerium in the large intestine of healthy mice *via* ICP-OES measurements; however, a significant amount of cerium was found in the large intestine of colitis mice (Figure 6C). Note that these values were obtained by performing ICP-OES on entire large intestines. Concentrations of cerium will be higher in the focal areas of diseased tissues. Furthermore, we investigated localization of Dex-CeNP in the large intestine of colitis mice *via* TEM. These micrographs revealed that Dex-CeNP accumulated in the large intestine of DSS-colitis mice that received Dex-CeNP (Figure 6D), which is not surprising, as dextran has an affinity for inflammatory disease

sites.[41] Also, it has been shown that activated macrophages in sites of inflammation actively uptake dextran nanoparticles *via* binding to macrophage scavenger receptors.[41–43]

Biodistribution

The biodistribution of Dex-CeNP was investigated in both healthy and DSS-induced colitis mice at 24 hrs post oral administration. The amounts of cerium in several organs, *i.e.* stomach, small intestine, large intestine, liver, spleen, heart, and kidneys, were measured *via* ICP-OES as presented in Figure S4. As can be seen, the biodistribution of Dex-CeNP in healthy mice was found to be slightly different to that observed in colitis mice. In the case of healthy mice, cerium was not found in any organ investigated, except the stomach, which had retained less than 0.04 % ID/g, indicating almost total clearance of Dex-CeNP at 24 hours, in agreement with the *in vivo* CT imaging results (Figure S3). However, small quantities of cerium were found in stomachs, small intestines and large intestines of colitis mice (0.4 %, 0.6 % and 1.4 %, respectively), each of which was statistically significantly greater than the values found in healthy mice (Figure S4). In addition, a very small amount of cerium was found in the spleen of the colitis animals (less than 0.1 % of the dose). Overall, 97.6 % of the dose was cleared from colitis animals at 24 hours. These ICP-OES results supported our observations from *in vivo* CT imaging that Dex-CeNP accumulated in the large intestine of colitis mice at 24 hrs post administration.

Histopathology

Histological changes in the stomach, small intestine and large intestine were investigated at 24 hrs post Dex-CeNP administration *via* H&E staining. Representative tissue micrographs are presented in Figure 7. No adverse effect was observed at 24 hrs post administration of Dex-CeNP. No obvious changes in cellularity or architecture were found in the tissues of the mice that received Dex-CeNP compared to the control mice (that received PBS), indicating the biocompatibility of Dex-CeNP.

Dex-CeNP generates strong CT contrast *in vitro* and *in vivo*, is biocompatible, protects cells from oxidative damage, and was cleared from the body within 24 hrs post administration without posing any serious adverse effects. The dextran coating resulted in improved water solubility, stability in physiological buffer and biocompatibility. Cerium oxide nanoparticles have been shown to protect against oxidation by scavenging free radicals generated from cells exposed to radiation. CT is an x-ray imaging technique that is more predominantly used for imaging GIT than to other medical imaging techniques. Cerium oxide nanoparticle CT contrast agents could also protect cells from x-ray radiation induced oxidative damage. Dex-CeNP was found to preferentially accumulate in sites of inflammation in the large intestine, a property that would make it very useful for imaging IBD with CT. Current CT contrast agents used in the clinic (*i.e.* iodinated small molecules) do not possess the aforementioned characteristics, *i.e.* specificity towards inflammation sites and protection against oxidation. Therefore, Dex-CeNP was found to be an effective CT contrast agent for imaging the GIT with IBD, and have potential to protect cells from radiation induced oxidative damage. In addition, Dex-CeNP represent a good candidate for an emerging CT modality, *i.e.* photon counting CT.

CT is a widely available and low cost imaging technique that is commonly used for abdominal imaging.[44] Compared with other techniques, such as MRI or nuclear imaging, it is rapid, has high spatial resolution and suffers fewer issues with bowel motion. In particular, MRI has issues for imaging the GIT due to tissue-gas interfaces.[45] Colonoscopy requires sedation and an onerous preparation procedure involving a clear liquid diet and taking laxatives.[46] Therefore, CT imaging agents specific for colitis imaging could be particularly valuable.

Previously, Wu *et al.* reported imaging colitis *via* intravenous injection of macrophages labeled with either iron oxide nanoparticles or In-111, which allowed imaging *via* MRI and SPECT, respectively.[47] Compared to the approach reported herein, as mentioned above, MRI and SPECT have drawbacks for imaging the GIT.[45] Moreover, the need to isolate cells, label them and inject them is cumbersome compared to an orally administered agent. Alternatively, there have been reports of fluorescence or luminescence based nanoparticle agents for colitis imaging.[48–50] While promising, optical imaging using external scanners is limited to structures less than 1 cm from the skin. Fluorescence imaging using devices similar to colonoscopy systems could be possible, but would also require the onerous prep of colonoscopy and such systems are not currently widely available. Therefore, the approach described herein, *i.e.* combining an orally administered agent with widely available CT imaging, has advantages compared with these previous reports.

Some studies have shown that cerium oxide nanoparticles have adverse effects on cells *in vitro* or small animals.[51, 52] However, it is worth noting that those studies were carried out with uncoated cerium oxide nanoparticles.[51, 52] Indeed, coating nanoparticles with a hydrophilic, biocompatible polymer such as dextran can improve biocompatibility. Dextran is not only very biocompatible but has also already been used in FDA approved nanoparticles.[20, 34] Therefore, the dextran coating of these cerium oxide nanoparticles is likely the reason for the improved cytocompatibility compared to some other studies.

CT is an x-ray based medical imaging technique that can cause free radical generation, with the possibility of adverse effects.[26, 27] In particular, IBD patients may receive many CT scans over their lifetimes. Since Dex-CeNP possesses ROS scavenger properties, using Dex-CeNP as a CT contrast agent could be beneficial for these patients. Despite the widespread study of nanoparticles as contrast agents for CT, surprisingly, there have been no prior reports of nanoparticle CT contrast agents used for IBD imaging. Therefore, our findings provide important advances in the nanoparticle CT contrast agent field. In addition, Dex-CeNP have good potential for clinical translation due to their favorable clearance profile.

The limitations of this study include the use of a small animal model of colitis as opposed to a larger animal model, which may better mimic human disease. Moreover, while we did not observe adverse effects from these agents, studies where repeated and higher doses are used, as well as longer term studies will be needed to definitively determine safety *in vivo*. In addition, protective effects against oxidative damage were not studied *in vivo*. Such topics will be the subject of future work. Furthermore, given the ROS scavenger properties of these nanoparticles, evaluation of their potential role as a theranostic agent for inflammatory diseases, such as colitis, will be of interest.

Conclusions

We successfully synthesized water soluble and biocompatible Dex-CeNP, which produced strong CT/SPCCT contrast and protected cells against oxidative damage *in vitro*. *In vivo* imaging results showed that Dex-CeNP produced strong CT contrast in the GIT and accumulated in tissues affected by colitis. ICP-OES and TEM confirmed the accumulation of Dex-CeNP in the large intestine of colitis mice at 24 hrs post administration. Notably, 99.9 % and 97.6% of oral doses were cleared from the body within 24 hrs in healthy mice and colitis mice, respectively. Therefore, Dex-CeNP has potential as a CT contrast agent for GIT imaging as well as imaging IBD.

Materials and Methods

Dex-CeNP synthesis

Dex-CeNP was synthesized *via* a precipitation method using ammonium hydroxide based on a protocol published elsewhere.[35, 53] In brief, 1 ml of 1 M cerium nitrate hexahydrate (Sigma-Aldrich, St. Louis, MO) was dissolved in 2 ml of 0.1 M dextran solution (Dextran T-10, Pharmacosmos, Holbaek, Denmark). Next, the mixture of cerium nitrate and dextran solution was added dropwise to a 20 ml glass vial containing 6 ml of concentrated ammonium hydroxide solution (28–30%, Sigma-Aldrich,) while stirring. Then the reaction mixture was heated to 90 °C for 1 hour. After 1 hour of heating, the reaction mixture was allowed to cool to room temperature and stirred overnight. The nanoparticle suspension was then spun at 4000 rpm for 10 minutes to remove large aggregates. The supernatant was transferred to ultra-filtration tubes (MWCO 100 kDa) for further washing with DI water. After several washes with DI water, the solvent was changed to PBS and then stored at 4 °C for future use.

Characterization

Hydrodynamic Diameter and Zeta Potential—The hydrodynamic diameter and zeta potential of Dex-CeNP was measured using a Nano-ZS 90 (Malvern Instrument, Malvern, UK). In brief, Dex-CeNP was diluted with DI water (75μl of Dex-CeNP from stock solution was diluted to 3 ml with DI water). From the diluted samples, 1.5 and 1 ml were used for the hydrodynamic diameter and zeta potential measurements, respectively.

Electron microscopy—Electron microscopy (EM) of Dex-CeNP was performed using a JEOL 1010 microscope operating at 80 kV. Diluted Dex-CeNP was dropped onto the EM grid (FCF-200-Cu, Electron Microscopy Sciences, Hatfield, PA) and the liquid was allowed to dry before microscopy was performed. High-resolution electron micrographs were collected using a JEOL 2010F microscope operating at 200 kV from Dex-CeNP mounted onto 200 mesh Cu grids with lacy carbon films.

UV-visible spectroscopy—UV-visible spectra of Dex-CeNP were recorded using a UV-visible spectrophotometer (Thermo-Fisher Scientific, USA). In brief, UV-visible spectra were obtained from 1 ml of diluted Dex-CeNP.

Powder X-ray diffraction—The X-ray diffraction (XRD) pattern of dried Dex-CeNP was recorded using a Rigaku GiegerFlex D/Max-B X-ray diffractometer in the range of 20° to 90°. The instrument was operated at 45 kV and 30 mA using a radiation wavelength of 1.54 and a scan rate of 2° per minute.

Fourier transform infra-red spectroscopy—Free dextran and Dex-CeNP were characterized using Fourier transform infra-red spectroscopy (FT-IR, JASCO FT/IR-480 PLUS, Easton, MD, USA) performed in transmission mode. The samples were processed by grinding with dry KBr and pressed into thin pellets.

Inductively coupled plasma optical emission spectroscopy—Inductively coupled plasma optical emission spectroscopy (ICP-OES) was used to measure the cerium concentrations in Dex-CeNP batches and also within tissue samples according to a protocol published elsewhere.[16] In brief, 10 μl of Dex-CeNP from the stock was placed in a 15 ml tube, and then 1 ml concentrated nitric acid followed by 200 μl hydrogen peroxide (30%) was added to tube. After complete dissolution of Dex-CeNP, the final volume in the tube was adjusted to 10 ml with DI water. The cerium concentration was measured using an ICP-OES system (Spectro Genesis ICP, Kleve, Germany).

Dex-CeNP phantom imaging with computed tomography

A Dex-CeNP phantom was constructed according to a protocol published elsewhere.[54] In brief, several concentrations from 0.5 to 10 mg/ml of Dex-CeNP, cerium nitrate hexahydrate (both normalized to the mass of cerium), iopamidol, and gold nanoparticles were made in DI water. From the stock of each concentration, 300 μl of each agent was placed into small plastic tubes and the tubes were secured in a plastic rack with parafilm. Next, the rack was placed in a plastic container, which was filled with water to 21 cm in height. The phantom was scanned with a clinical CT scanner (Siemens SOMATOM Force 192-slice, Erlangen, Germany). CT images were acquired at 80, 100, 120 and 140 kV tube voltages, with a slice thickness of 0.5 mm, matrix size of 512 × 512, and field of view 37 × 37 cm. The x-ray tube current was 360 mA for each tube voltage and convolution kernel Br 40d was used. The images were analyzed using Osirix MD 64 bit software. The CT attenuation value in Hounsfield units (HU) for each sample tube was recorded from three different slices and averaged for each concentration. The data are presented as average CT attenuation values in HU and CT attenuation rates (HU.ml/mg) of different agents. Error bars represent the standard deviations. Samples were also scanned with a microCT system (Molecubes, Ghent, Belgium). CT images were acquired using the following parameters, slice thickness 100 μm, field of view 100 mm, tube voltage 50 kV, tube current 100 μA, and iterative reconstruction kernel. Images were analyzed as above. Spectral photon-counting CT images were acquired at 120 kV tube voltage, 100 mAs tube current and reconstructed with a slice thickness of 0.25 mm. A maximum-likelihood based material decomposition of the attenuation was used to generate two spectral material images, *i.e.* cerium and water, both scaled in mg/ml, allowing measurements of the concentration of each specific material. Conventional images were also reconstructed for HU visualization such as for conventional CT. Further technical details concerning the SPCCT system are provided in a previous study.[55]

In vitro cell viability

Cell Culture—HepG2 (human hepatocellular liver carcinoma), BJ5ta (human fibroblast), C2BBe1 (human colorectal adenocarcinoma, epithelial) and J774A.1 (murine macrophage) cells were purchased from ATCC (Manassas, VA, USA). HepG2 cells were maintained in a culture medium of Eagle's Minimum Essential Medium (EMEM, Gibco, Grand Island, NY USA), 10% FBS, 45 IU/ml penicillin and 45 IU/ml streptomycin (Gibco). BJ5ta cells were maintained in a culture medium containing 4 parts of Dulbecco's Modified Eagle's Medium (DMEM), 1 part of medium 199, 10 % fetal bovine serum (FBS) (Gibco) and 0.01 mg/ml of hygromycin B (Sigma-Aldrich). C2BBe1 and J774A.1 cells were maintained in a culture medium of DMEM, 10% FBS, 45 IU/ml penicillin and 45 IU/ml streptomycin (Gibco), with 10 μg/ml human transferrin (Sigma-Aldrich) added to the C2BBe1 culture medium. The cells were grown at 37 °C in 5% CO_2 humidified incubator.

Cell viability assay—The cytotoxicity of Dex-CeNP was analyzed using the MTS ((3-(4,5-dimethylthiazol-2-yl)-5-(3-carboxymethoxyphenyl)-2-(4-sulfophenyl)-2*H*-tetrazolium)) assay (CellTiter 96 cell proliferation assay kit; Promega, Madison, WI, USA). The assay was performed in 96 well flat bottom microplates (Corning, NY, USA), according to previously published methods.[18] Three independent experiments were performed for each concentration. The percentage of relative cell viability was calculated compared to control and the data presented as mean ± standard deviation (n= 3).

Protective effect of Dex-CeNP against oxidative damage

The protective effect of Dex-CeNP against oxidative damage was investigated in two different cell types, *i.e.* C2BBe1 and BJ5ta cells. The assay was performed in 96 well flat bottom microplates. In brief, 10,000 cells in 100 μl of cell culture media were added to each well of a 96 well plate, and then the 96 well plate was incubated in a CO_2 incubator for 24 hrs. After 24 hrs, the cells were washed with sterile PBS gently, and incubated with Dex-CeNP, hydrogen peroxide or Dex-CeNP/hydrogen peroxide for 30 minutes. After 30 minutes, the cell culture media from each well was discarded, the cells washed with sterile PBS, 100 μl of fresh cell culture media added to each well, and then incubated in a CO_2 incubator for 24 hrs. At this point, cell viability was measured using the MTS assay (described above in the 'cell viability assay' section). The percentage of relative cell viability was calculated compared to control and the data presented as mean ± standard deviation (n= 3). The exposure concentration of hydrogen peroxide was 0.075 % and 0.0125 % for C2BBe1 and BJ5ta cells respectively, while the Dex-CeNP exposure concentration was the same for both cell types, *i.e.* 0.5 mg/ml. The exposure concentration of hydrogen peroxide was different for C2BBe1 and BJ5ta cells, as their sensitivity to hydrogen peroxide was found to be different.

In vivo characterization of Dex-CeNP

Animal experiments—*In vivo* experimental protocols were approved by the Institutional Animal Care and Use Committee (IACUC) of the University of Pennsylvania and were carried out in accordance with all national or local guidelines and regulations. 7 weeks old

C57BL/6 male and female mice were purchased from Jackson laboratory (Bar Harbor, Maine, USA).

Acute dextran sodium sulfate colitis model—Acute dextran sodium sulfate colitis (DSS-colitis) in mice was developed using dextran sodium sulfate (DSS) according a published protocol.[56] On day 1, mice were weighed and numbered. The water supply of the mouse cages was filled with 2 % (w/v) DSS (molecular weight: 36,000–50,000 Da, MP Biomedicals, Irvine, CA) to induce colitis. Control mice received the same drinking water without DSS. On day 3, the remaining DSS solution was removed from the cage water bottles, which were refilled with fresh DSS solution. On day 5, the remaining DSS solution was removed from the cage water bottles and was refilled with fresh DSS solution. On day 8, the remaining DSS solution was replaced by autoclaved water. After 8 days of DSS treatment, the mice developed colitis in their large bowel.

In vivo imaging—*In vivo* imaging experiments were performed with a microCT (Molecubes, Gent, Belgium). Imaging experiments were performed using mice with and without colitis (n = 6 per group, in each group 3 male and 3 female mice were used). In brief, mice with or without colitis were scanned with microCT, and then either Dex-CeNP or iopamidol was administered *via* gavage. The dose for Dex-CeNP or iopamidol was 250 mg Ce or I /kg body weight. After Dex-CeNP or iopamidol administration, mice were scanned at 5 minutes, 30 minutes, 60 minutes, 120 minutes, and 24 hrs. CT images were acquired using the following parameters, slice thickness 100 μm, field of view 100 mm, tube voltage 50 kV, tube current 100 μA, and iterative reconstruction kernel. The CT images were analyzed using Osirix MD 64 bit software. The attenuation values in Hounsfield units (HU) for stomach, small intestine and large intestine were recorded from three different slices and averaged. The data is presented as the change in attenuation compared to pre-injection scan (mean ± SD). Error bars are standard deviations.

Biodistribution—The biodistribution of Dex-CeNP was investigated in mice with or without DSS-induced colitis and in each group 6 mice (3 male and 3 female) were used. At 24 hrs post Dex-CeNP administration, the mice were sacrificed and perfused *via* the left ventricle with 20 ml PBS. The liver, spleen, heart, stomach, small intestine, and large intestine were collected. The stomach, small intestine and large intestine were flushed with PBS to remove food materials. Next, the mass of each tissue was recorded, and the organs were cut into small pieces. These tissue samples were transferred to glass tubes; 1 ml of concentrated nitric acid was added to each tube and then incubated in an oven at 75 °C for 16 hrs. Next, 200 μl of concentrated hydrogen peroxide (30%) was added to each tube to dissolve cerium oxide nanoparticles. After addition of hydrogen peroxide, the tubes were incubated at 37 °C for another 2 hrs. Next, the volume in each tube was made to 10 ml with DI water, prior to analyze the cerium concentration with ICP-OES. The result was presented as mean ± SD. Error bars are standard deviations.

Electron microscopy on tissue samples—Large intestine tissue samples from DSS-induced colitis mice were acquired at 24 hrs post administration of Dex-CeNP. Tissues were washed with cold PBS and then fixed in 2.5 % glutaraldehyde and 2 % paraformaldehyde in

0.1 M sodium cacodylate buffer (pH 7.4) overnight at 4 °C. After subsequent buffer washes, the samples were fixed with 2 % osmium tetroxide for 1 hr at room temperature. After 1 hr, samples were rinsed with DI water prior to *en bloc* staining with 2 % uranyl acetate. Next, samples were dehydrated using graded ethanol series. The tissue was then infiltrated and embedded in EMbed-812 (Electron Microscopy Sciences, Fort Washington, PA). The embedded tissue samples were sectioned using a DiATOME diamond knife. Thin sections were stained with uranyl acetate and lead citrate, and examined with a JEOL 1010 electron microscope.

Histopathology—Histological investigation on tissue samples from stomachs, small intestines and large intestines was performed at 24 hrs post administration of Dex-CeNP or PBS (as a negative control). Tissue samples (*i.e.* stomach, small intestine and large intestine) were harvested, washed with cold PBS, and then cut into small pieces. Next, samples were fixed in 10% neutral buffered formalin, and then dehydrated with ethanol. After dehydration, tissue samples were embedded in paraffin, sectioned, and then stained with hematoxylin and eosin (H&E). After staining, images were acquired with a Leica DM4000B upright microscope paired with a Spot RT/SE slider camera.

Statistics:

All the experiments mentioned above were performed in triplicate (three independent experiments). Statistical analysis was carried out *via* two-sample Student's *t*-tests (unequal variance) and ANOVA tests using STATA 16 software.

Supplementary Material

Refer to Web version on PubMed Central for supplementary material.

Acknowledgements

This work was supported by funding from NIH grant R01-HL131557 (DPC), NSF Graduate Fellowship DGE-845298 (JCH), American Heart Association grant 18PRE34030383 (JK) and a Franco-American Commission Fulbright fellowship (MB). We acknowledge Eric Blankemeyer from Radiology Department of University of Pennsylvania for his help with the microCT scans. We thank Portia Maidment for her feedback on the manuscript.

References

1. Cai QY; Kim SH; Choi KS; Kim SY; Byun SJ; Kim KW; Park SH; Juhng SK; Yoon KH Colloidal Gold Nanoparticles as a Blood-Pool Contrast Agent for X-Ray Computed Tomography in Mice. Invest. Radiol 2007, 42, 797–806. [PubMed: 18007151]
2. Chhour P; Naha PC; O'Neill SM; Litt HI; Reilly MP; Ferrari VA; Cormode DP Labeling Monocytes with Gold Nanoparticles to Track Their Recruitment in Atherosclerosis with Computed Tomography. Biomaterials 2016, 87, 93–103. [PubMed: 26914700]
3. Cormode DP; Naha P; Fayad ZA Nanoparticle Contrast Agents for Computed Tomography: A Focus on Micelles. Contrast Media Mol. Imaging 2014, 9, 37–52. [PubMed: 24470293]
4. Kilcoyne A; Kaplan JL; Gee MS Inflammatory Bowel Disease Imaging: Current Practice and Future Directions. World J. Gastroenterol 2016, 22, 917–932. [PubMed: 26811637]
5. Maglinte DDT; Sandrasegaran K; Lappas JC; Chiorean M CT Enteroclysis. Radiology 2007, 245, 661–671. [PubMed: 18024448]
6. Eliakim R; Magro F Imaging Techniques in IBD and Their Role in Follow-Up and Surveillance. Nat. Rev. Gastroenterol. Hepatol 2014, 11, 722. [PubMed: 25157623]

7. Viscido A; Capannolo A; Latella G; Caprilli R; Frieri G Nanotechnology in the Treatment of Inflammatory Bowel Diseases. J. Crohns Colitis 2014, 8, 903–918. [PubMed: 24686095]
8. Si-Mohamed S; Thivolet A; Bonnot P-E; Bar-Ness D; Kepenekian V; Cormode DP; Douek P; Rousset P Improved Peritoneal Cavity and Abdominal Organ Imaging Using a Biphasic Contrast Agent Protocol and Spectral Photon Counting CT. Invest. Radiol 2018, 53, 629–639. [PubMed: 29794948]
9. Winklhofer S; Lin W-C; Wang ZJ; Behr SC; Westphalen AC; Yeh BM Comparison of Positive Oral Contrast Agents for Abdominopelvic CT. Am. J. Roentgenol 2019, 212, 1037–1043.
10. FitzGerald PF; Colborn RE; Edic PM; Lambert JW; Torres AS; Bonitatibus PJ; Yeh BM CT Image Contrast of High-Z Elements: Phantom Imaging Studies and Clinical Implications. Radiology 2016, 278, 723–733. [PubMed: 26356064]
11. Lambert JW; Sun Y; Stillson C; Li Z; Kumar R; Wang S; FitzGerald PF; Bonitatibus PJ; Colborn RE; Roberts JC; Edic PM; Marino M; Yeh BM, An Intravascular Tantalum Oxide–Based CT Contrast Agent: Preclinical Evaluation Emulating Overweight and Obese Patient Size. Radiology 2018, 289, 103–110. [PubMed: 29969071]
12. Sbitany H; Koltz PF; Mays C; Girotto JA; Langstein HN CT Contrast Extravasation in the Upper Extremity: Strategies for Management. Int. J. Surg 2010, 8, 384–386. [PubMed: 20541631]
13. Smith-Bindman R; Lipson J; Marcus R; Kim K-P; Mahesh M; Gould R; Berrington de González A; Miglioretti DL Radiation Dose Associated with Common Computed Tomography Examinations and the Associated Lifetime Attributable Risk of Cancer. Arch. Intern. Med 2009, 169, 2078–2086. [PubMed: 20008690]
14. Cormode DP; Skajaa T; van Schooneveld MM; Koole R; Jarzyna P; Lobatto ME; Calcagno C; Barazza A; Gordon RE; Zanzonico P; Fisher EA; Fayad ZA; Mulder WJ Nanocrystal Core High-Density Lipoproteins: A Multimodality Contrast Agent Platform. Nano Lett. 2008, 8, 3715–3723. [PubMed: 18939808]
15. Hsu JC; Naha PC; Lau KC; Chhour P; Hastings R; Moon BF; Stein JM; Witschey WRT; McDonald ES; Maidment ADA; Cormode DP An All-In-One Nanoparticle (AION) Contrast Agent for Breast Cancer Screening with DEM-CT-MRI-NIRF Imaging. Nanoscale 2018, 10, 17236–17248. [PubMed: 30191237]
16. Naha PC; Lau KC; Hsu JC; Hajfathalian M; Mian S; Chhour P; Uppuluri L; McDonald ES; Maidment ADA; Cormode DP Gold Silver Alloy Nanoparticles (GSAN): An Imaging Probe for Breast Cancer Screening with Dual-Energy Mammography or Computed Tomography. Nanoscale 2016, 8, 13740–13754. [PubMed: 27412458]
17. Brown AL; Naha PC; Benavides-Montes V; Litt HI; Goforth AM; Cormode DP Synthesis, X-ray Opacity, and Biological Compatibility of Ultra-High Payload Elemental Bismuth Nanoparticle X-Ray Contrast Agents. Chem. Mater 2014, 26, 2266–2274. [PubMed: 24803727]
18. Naha PC; Chhour P; Cormode DP Systematic In Vitro Toxicological Screening of Gold Nanoparticles Designed for Nanomedicine Applications. Toxicol. In Vitro 2015, 29, 1445–1453. [PubMed: 26031843]
19. Dong YC; Hajfathalian M; Maidment PSN; Hsu JC; Naha PC; Si-Mohamed S; Breuilly M; Kim J; Chhour P; Douek P; Litt HI; Cormode DP Effect of Gold Nanoparticle Size on Their Properties as Contrast Agents for Computed Tomography. Sci. Rep 2019, 9, 14912. [PubMed: 31624285]
20. Naha PC; Liu Y; Hwang G; Huang Y; Gubara S; Jonnakuti V; Simon-Soro A; Kim D; Gao L; Koo H; Cormode DP Dextran-Coated Iron Oxide Nanoparticles as Biomimetic Catalysts for Localized and pH-Activated Biofilm Disruption. ACS Nano 2019, 13, 4960–4971. [PubMed: 30642159]
21. Hu G; Guo M; Xu J; Wu F; Fan J; Huang Q; Yang G; Lv Z; Wang X; Jin Y Nanoparticles Targeting Macrophages as Potential Clinical Therapeutic Agents against Cancer and Inflammation. Front. Immunol 2019, 10, 1998. [PubMed: 31497026]
22. Caputo F; De Nicola M; Sienkiewicz A; Giovanetti A; Bejarano I; Licoccia S; Traversa E; Ghibelli L Cerium Oxide Nanoparticles, Combining Antioxidant and UV Shielding Properties, Prevent UV-Induced Cell Damage and Mutagenesis. Nanoscale 2015, 7, 15643–15656. [PubMed: 26349675]
23. Baldim V; Bedioui F; Mignet N; Margaill I; Berret JF, The Enzyme-Like Catalytic Activity of Cerium Oxide Nanoparticles and Its Dependency on Ce3+ Surface Area Concentration. Nanoscale 2018, 10, 6971–6980. [PubMed: 29610821]

24. Kim CK; Kim TK; Choi IY; Soh M; Kim D; Kim YJ; Jang H; Yang HS; Kim JY; Park HK; Park SP; Park S; Yu T; Yoon BW; Hyeon T Ceria Nanoparticles That Can Protect against Ischemic Stroke. Angew. Chem 2012, 51, 11039–11043. [PubMed: 22968916]
25. Genchi GG; Marino A; Grillone A; Pezzini I; Ciofani G Remote Control of Cellular Functions: The Role of Smart Nanomaterials in the Medicine of the Future. Adv. Healthcare Mater 2017, 6, 1700002.
26. Nie J; Peng C; Pei W; Zhu W; Zhang S; Cao H; Qi X; Tong J; Jiao Y A Novel Role of Long Non-Coding RNAs in Response to X-Ray Irradiation. Toxicol. In Vitro 2015, 30, 536–544. [PubMed: 26363204]
27. Cervelli T; Panetta D; Navarra T; Gadhiri S; Salvadori P; Galli A; Caramella D; Basta G; Picano E; Del Turco S A New Natural Antioxidant Mixture Protects against Oxidative and DNA Damage in Endothelial Cell Exposed to Low-Dose Irradiation. Oxid. Med. Cell Longevity 2017, 9085947.
28. Das S; Dowding JM; Klump KE; McGinnis JF; Self W; Seal S Cerium Oxide Nanoparticles: Applications and Prospects in Nanomedicine. Nanomedicine 2013, 8, 1483–1508. [PubMed: 23987111]
29. Celardo I; Pedersen JZ; Traversa E; Ghibelli L Pharmacological Potential of Cerium Oxide Nanoparticles. Nanoscale 2011, 3, 1411–1420. [PubMed: 21369578]
30. Celardo I; Traversa E; Ghibelli L Cerium Oxide Nanoparticles: A Promise for Applications in Therapy. J. Exp. Ther. Oncol 2011, 9, 47–51. [PubMed: 21275265]
31. Xu PT; Maidment BW 3rd; Antonic V; Jackson IL; Das S; Zodda A; Zhang X; Seal S; Vujaskovic Z Cerium Oxide Nanoparticles: A Potential Medical Countermeasure to Mitigate Radiation-Induced Lung Injury in CBA/J Mice. Radiat. Res 2016, 185, 516–526. [PubMed: 27135969]
32. Celardo I; De Nicola M; Mandoli C; Pedersen JZ; Traversa E; Ghibelli L Ce(3)+ Ions Determine Redox-Dependent Anti-Apoptotic Effect of Cerium Oxide Nanoparticles. ACS Nano 2011, 5, 4537–4549. [PubMed: 21612305]
33. Hijaz M; Das S; Mert I; Gupta A; Al-Wahab Z; Tebbe C; Dar S; Chhina J; Giri S; Munkarah A; Seal S; Rattan R Folic Acid Tagged Nanoceria as a Novel Therapeutic Agent in Ovarian Cancer. BMC Cancer 2016, 16, 220–220. [PubMed: 26979107]
34. Naha P; Al-Zaki A; Hecht ER; Chorny M; Chhour P; Blankemeyer E; Yates DM; Witschey WRT; Litt HI; Tsourkas A; Cormode DP Dextran Coated Bismuth-Iron Oxide Nanohybrid Contrast Agents for Computed Tomography and Magnetic Resonance Imaging. J. Mater. Chem. B 2014, 2, 8239–8248. [PubMed: 25485115]
35. Perez JM; Asati A; Nath S; Kaittanis C Synthesis of Biocompatible Dextran-Coated Nanoceria with pH-Dependent Antioxidant Properties. Small 2008, 4, 552–556. [PubMed: 18433077]
36. Seymour FR; Julian RL; Jeanes A; Lamberts BL, Structural Analysis of Insoluble D-Glucans by Fourier-Transform, Infrared Difference-Spectrometry: Correlation Between Structures of Dextrans from Strains of Leuconostoc Mesenteroides and of D-Glucans from Strains of Streptococcus Mutans. Carbohydr. Res 1980, 86, 227–246.
37. Shingel KI Determination of Structural Peculiarities of Dextran, Pullulan and γ-Irradiated Pullulan by Fourier-Transform IR Spectroscopy. Carbohydr. Res 2002, 337, 1445–1451. [PubMed: 12204605]
38. Genchi GG; Marino A; Grillone A; Pezzini I; Ciofani G Remote Control of Cellular Functions: The Role of Smart Nanomaterials in the Medicine of the Future. Adv. Healthcare Mater 2017, 6, 1700002.
39. Heckert EG; Karakoti AS; Seal S; Self WT The Role of Cerium Redox State in the SOD Mimetic Activity of Nanoceria. Biomaterials 2008, 29, 2705–2709. [PubMed: 18395249]
40. Pirmohamed T; Dowding JM; Singh S; Wasserman B; Heckert E; Karakoti AS; King JES; Seal S; Self WT Nanoceria Exhibit Redox State-Dependent Catalase Mimetic Activity. Chem. Commun. (Cambridge, U. K.) 2010, 46, 2736–2738.
41. Lo TN; Almeida AP; Beaven MA Dextran and Carrageenan Evoke Different Inflammatory Responses in Rat with Respect to Composition of Infiltrates and Effect of Indomethacin. J. Pharmacol. Exp. Ther 1982, 221, 261–267. [PubMed: 6174730]

42. Kim S-H; Kim J-H; You DG; Saravanakumar G; Yoon HY; Choi KY; Thambi T; Deepagan VG; Jo D-G; Park JH Self-Assembled Dextran Sulphate Nanoparticles for Targeting Rheumatoid Arthritis. Chem. Commun. (Cambridge, U. K.) 2013, 49, 10349–10351.
43. Yang M; Ding J; Feng X; Chang F; Wang Y; Gao Z; Zhuang X; Chen X, Scavenger Receptor-Mediated Targeted Treatment of Collagen-Induced Arthritis by Dextran Sulfate-Methotrexate Prodrug. Theranostics 2017, 7, 97–105. [PubMed: 28042319]
44. Deepak P; Bruining DH Radiographical Evaluation of Ulcerative Colitis. Gastroenterol. Rep. (Oxf) 2014, 2, 169–177. [PubMed: 24843072]
45. Wu Y; Briley K; Tao X, Nanoparticle-Based Imaging of Inflammatory Bowel Disease. Wiley Interdiscip. Rev.: Nanomed. Nanobiotechnol 2016, 8, 300–315. [PubMed: 26371464]
46. Parra-Blanco A; Ruiz A; Alvarez-Lobos M; Amorós A; Gana JC; Ibáñez P; Ono A; Fujii T Achieving the Best Bowel Preparation for Colonoscopy. World J. Gastroenterol 2014, 20, 17709–17726. [PubMed: 25548470]
47. Wu Y; Briley-Saebo K; Xie J; Zhang R; Wang Z; He C; Tang CY; Tao X Inflammatory Bowel Disease: MR- and SPECT/CT-Based Macrophage Imaging for Monitoring and Evaluating Disease Activity in Experimental Mouse Model--Pilot Study. Radiology 2014, 271, 400–407. [PubMed: 24475849]
48. Poh S; Putt KS; Low PS Folate-Targeted Dendrimers Selectively Accumulate at Sites of Inflammation in Mouse Models of Ulcerative Colitis and Atherosclerosis. Biomacromolecules 2017, 18, 3082–3088. [PubMed: 28863264]
49. Guo J; Tao H; Dou Y; Li L; Xu X; Zhang Q; Cheng J; Han S; Huang J; Li X; Li X; Zhang J A Myeloperoxidase-Responsive and Biodegradable Luminescent Material for Real-Time Imaging of Inflammatory Diseases. Mater. Today 2017, 493–500.
50. Zhou Y; Yang S; Guo J; Dong H; Yin K; Huang WT; Yang R *In Vivo* Imaging of Hypoxia Associated with Inflammatory Bowel Disease by a Cytoplasmic Protein-Powered Fluorescence Cascade Amplifier. Anal. Chem 2020, 92, 5787–5794.
51. Nemmar A; Al-Salam S; Beegam S; Yuvaraju P; Ali BH Aortic Oxidative Stress, Inflammation and DNA Damage Following Pulmonary Exposure to Cerium Oxide Nanoparticles in a Rat Model of Vascular Injury. Biomolecules 2019, 9, E376. [PubMed: 31426470]
52. Guo C; Robertson S; Weber RJM; Buckley A; Warren J; Hodgson A; Rappoport JZ; Ignatyev K; Meldrum K; Romer I; Macchiarulo S; Chipman JK; Marczylo T; Leonard MO; Gant TW; Viant MR; Smith R Pulmonary Toxicity of Inhaled Nano-Sized Cerium Oxide Aerosols in Sprague-Dawley Rats. Nanotoxicology 2019, 13, 733–750. [PubMed: 30704321]
53. Alpaslan E; Yazici H; Golshan NH; Ziemer KS; Webster TJ pH-Dependent Activity of Dextran-Coated Cerium Oxide Nanoparticles on Prohibiting Osteosarcoma Cell Proliferation. ACS Biomater. Sci. Eng 2015, 1, 1096–1103.
54. Zhang G; Naha PC; Gautam P; Cormode DP; Chan JMW Water-Dispersible Bismuth–Organic Materials with Computed Tomography Contrast Properties. ACS Appl. Bio Mater 2018, 1, 1918–1926.
55. Si-Mohamed S; Bar-Ness D; Sigovan M; Tatard-Leitman V; Cormode DP; Naha PC; Coulon P; Rascle L; Roessl E; Rokni M; Altman A; Yagil Y; Boussel L; Douek P Multicolour Imaging with Spectral Photon-Counting CT: A Phantom Study. Eur. Radiol. Exp 2018, 2, 34. [PubMed: 30327898]
56. Wirtz S; Popp V; Kindermann M; Gerlach K; Weigmann B; Fichtner-Feigl S; Neurath MF Chemically Induced Mouse Models of Acute and Chronic Intestinal Inflammation. Nat. Protoc 2017, 12, 1295. [PubMed: 28569761]

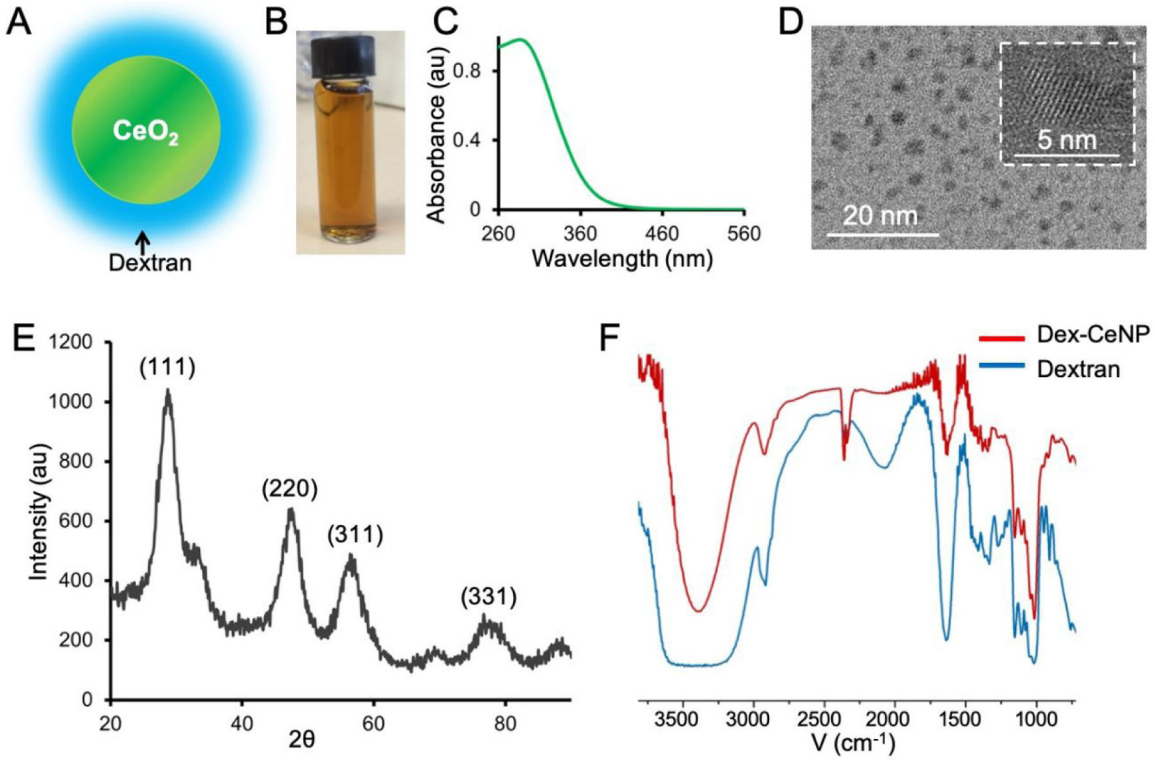

Figure 1.

Characterization of Dex-CeNP. A) Schematic depiction of Dex-CeNP. B) Photograph of Dex-CeNP suspended in PBS. C) UV-visble spectrum of Dex-CeNP. D) Transmission electron micrograph (TEM) of Dex-CeNP. HR-TEM of a Dex-CeNP is shown in the white boxed area. E) XRD pattern of Dex-CeNP. F) Fourier transform infra-red (FT-IR) spectra of dextran (blue line) and Dex-CeNP (red line).

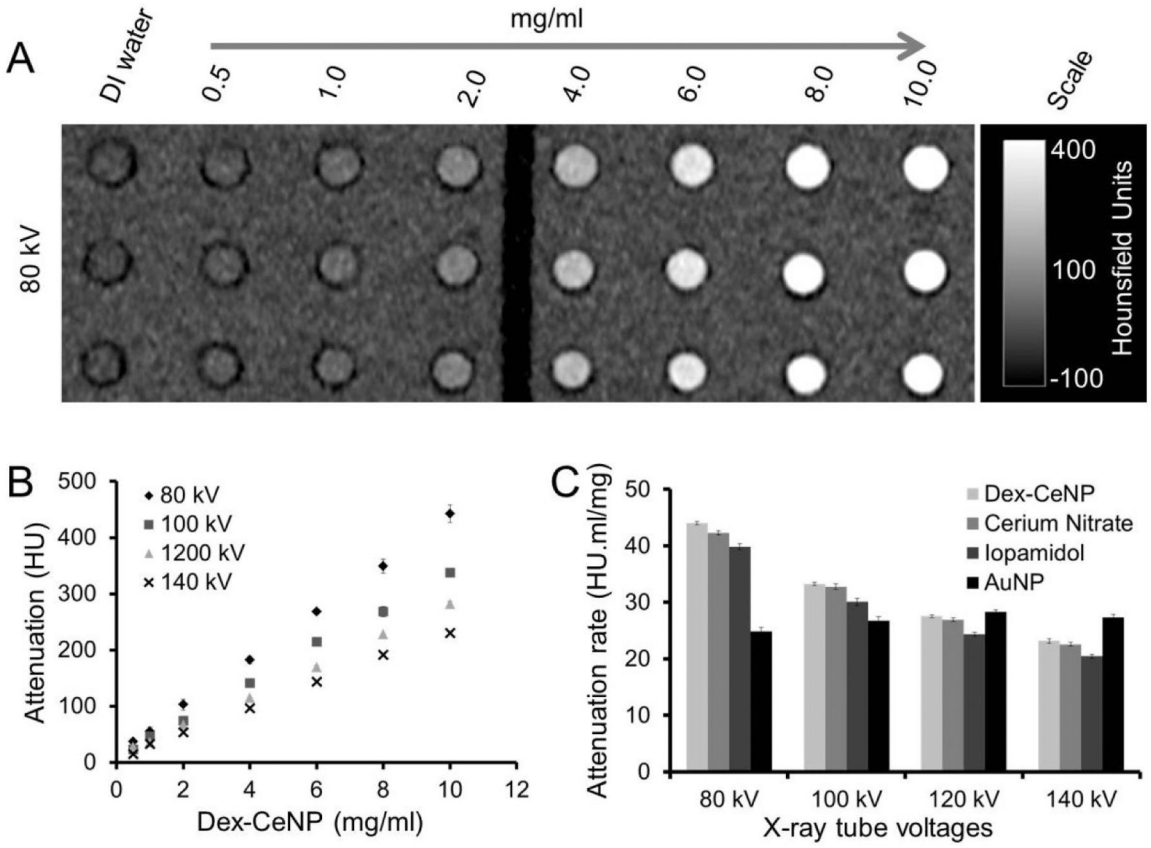

Figure 2.

Contrast generation from a Dex-CeNP phantom scanned with a clinical CT system. A) A representative Dex-CeNP phantom image acquired at 80 kV. B) X-ray attenuation *versus* mass concentration of cerium when Dex-CeNP were scanned with different tube voltages. Error bars are standard deviations. Some error bars are not visible as they are obscured by the data point. C) X-ray attenuation rates of different contrast agents. Error bars represent standard errors.

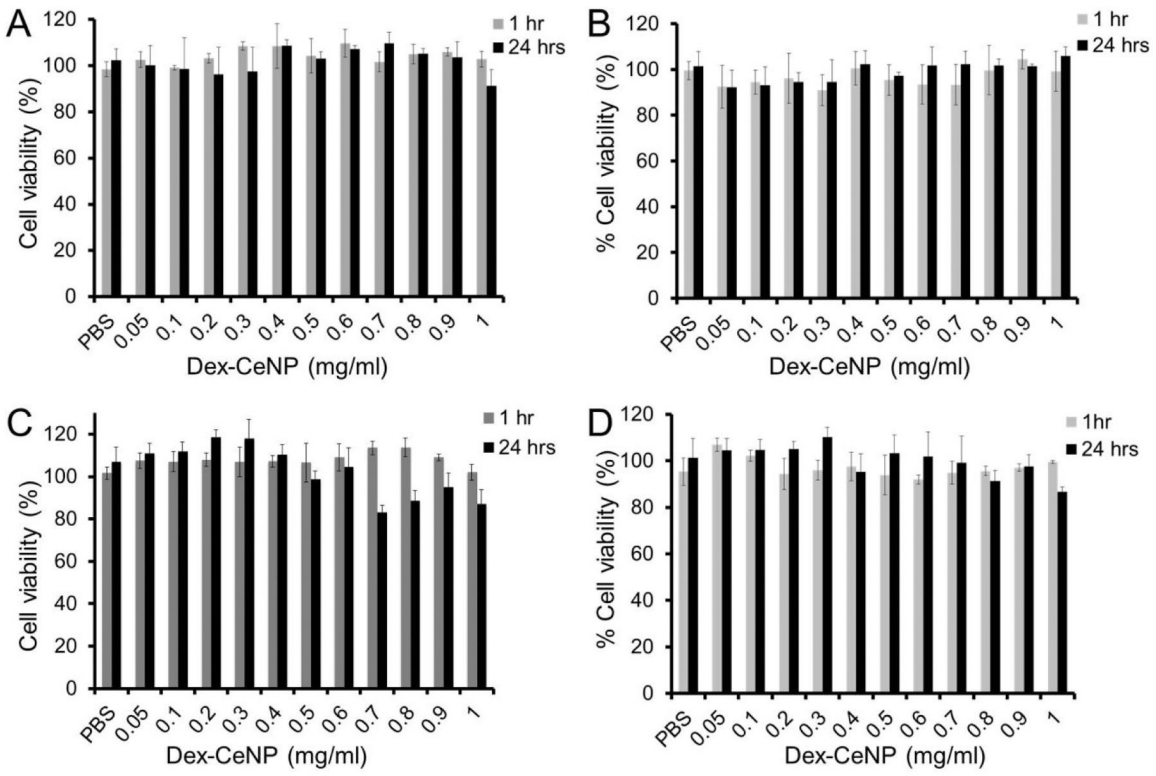

Figure 3.

Effect of Dex-CeNP on the viability of A) BJ5ta cells, B) J774A.1 cells, C) C2BBe1 cells, and D) HepG2 cells. Data shown as mean ± SD. Three independent experiments were performed (n=3).

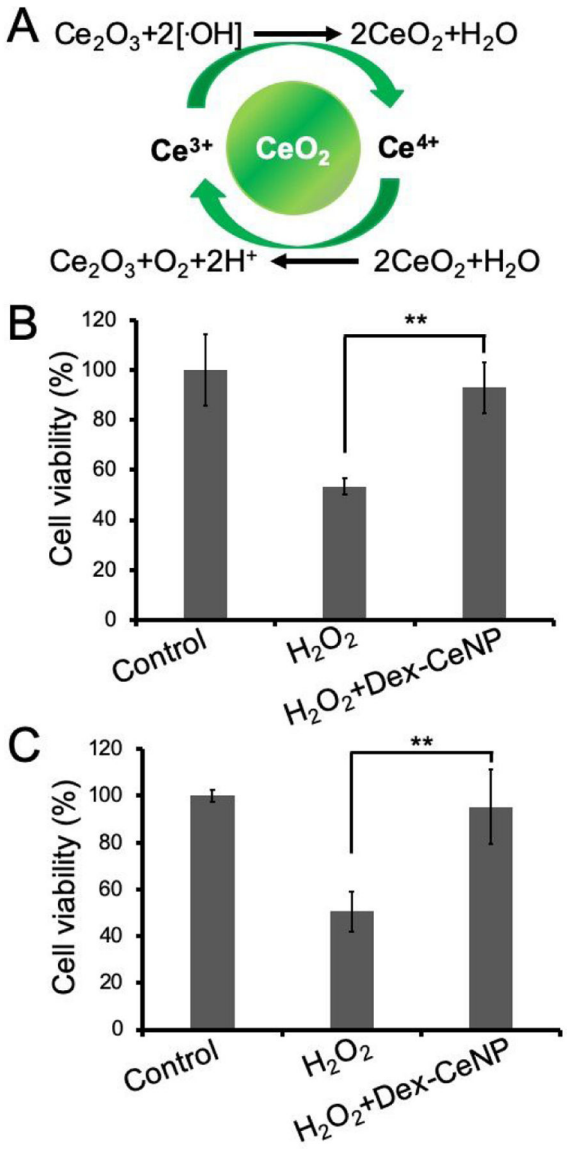

Figure 4.

The protective effect of Dex-CeNP against hydrogen peroxide induced oxidative damage in cells. A) Schematic showing cerium oxide nanoparticles neutralizing hydroxyl free radicals *via* an oxidation-reduction cycle. Dex-CeNP protected B) C2BBe1 and C) BJ5ta cells from hydrogen peroxide exposure (0.075% and 0.0125%, respectively). Data presented as mean ± SD. Three independent experiments were performed (n=3). ** indicates statistically significant difference at $p < 0.01$.

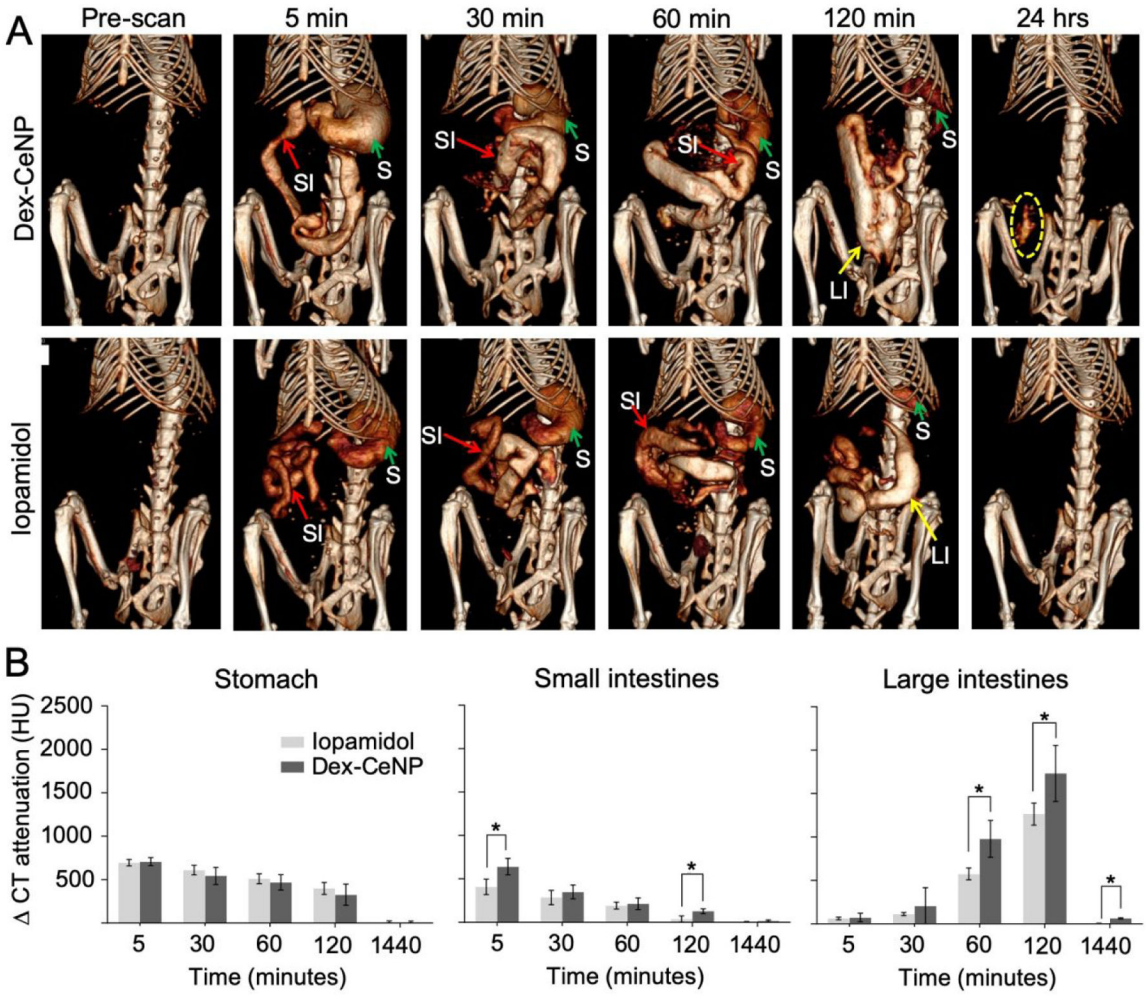

Figure 5.

In vivo CT imaging of DSS-induced colitis mice administered Dex-CeNP or iopamidol. A) Representative micro-CT images of colitis mice, pre and post oral administration of Dex-CeNP or iopamidol. ‘S’ indicates the stomach, ‘SI’ indicates the small intestine, and ‘LI’ indicates the large intestine. The yellow dashed oval indicates Dex-CeNP accumulation in an area of colitis. B) CT attenuation in the GIT arising from administration of either Dex-CeNP or iopamidol. Y-axis scale is the same for each graph. For each treatment group six mice (3 male and 3 female) were used. * indicates statistically significant differences at $p < 0.05$.

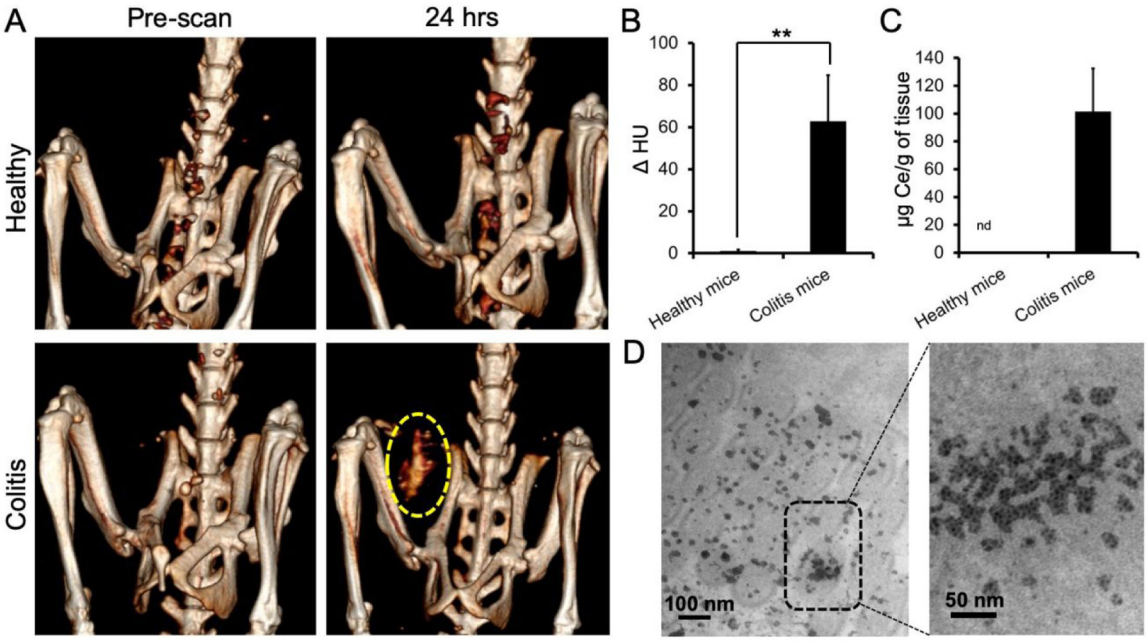

Figure 6:

Dex-CeNP accumulated in the inflamed large intestines of DSS-colitis mice. A) Representative CT images of healthy or colitis mice at pre and 24 hrs post oral administration of Dex-CeNP. The yellow dashed oval indicates CT contrast from Dex-CeNP accumulated in the colitis affected region at 24 hrs. B) Graph showing CT attenuation in the large intestines of healthy and DSS-colitis mice at the 24 hr time point. C) Cerium content in the large intestines of healthy and colitis mice at 24 hrs post administration of Dex-CeNP. In B and C, the data are presented as mean ± SD. D) Representative electron micrographs of a large intestine from a DSS-colitis mouse showing accumulation of nanoparticles at 24 hrs. For each treatment group six mice (3 male and 3 female) were used. ** indicates statistically significant differences at $p < 0.01$.

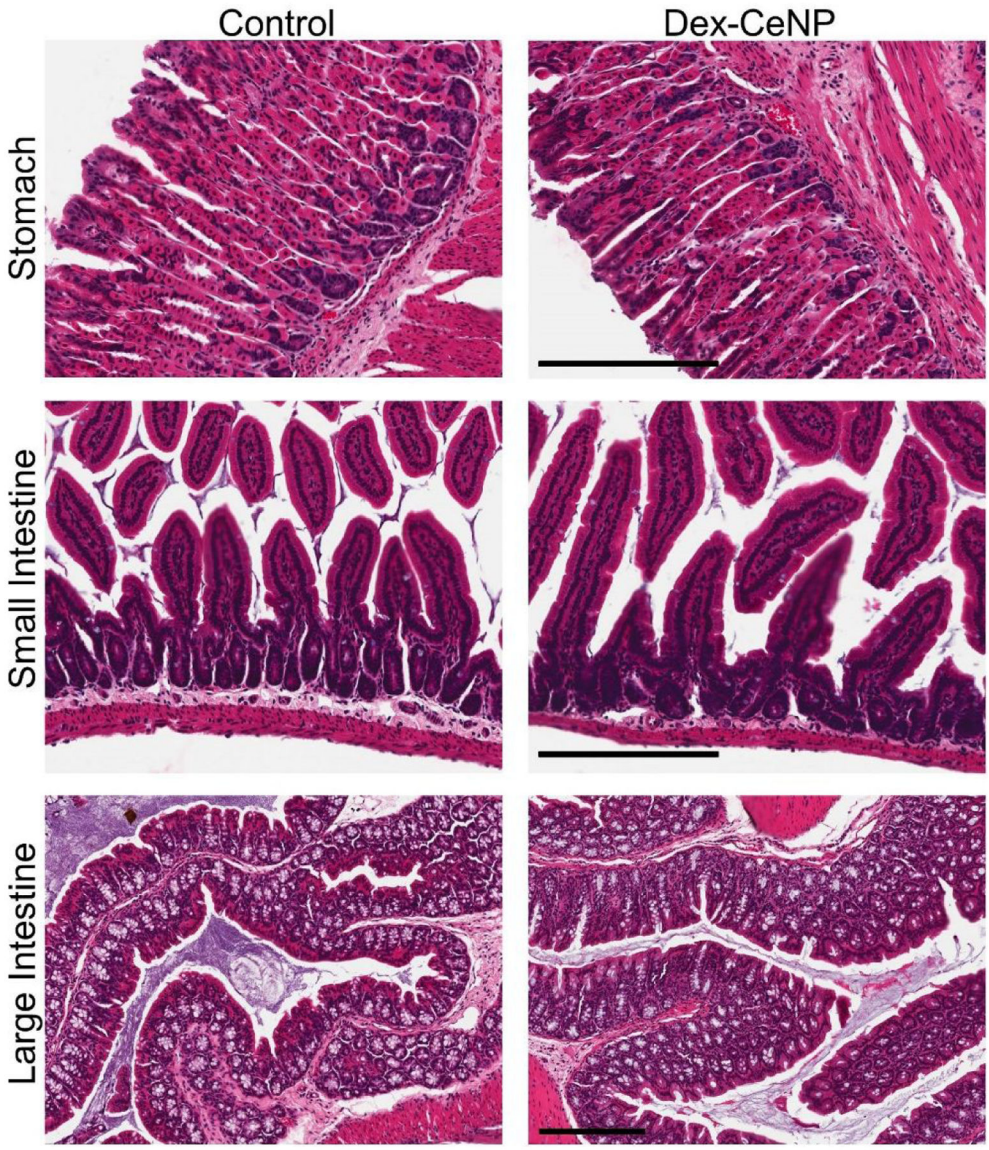

Figure 7.

Histology of stomachs, small intestines and large intestines of healthy mice at 24 hrs post Dex-CeNP or PBS administration. Scale bar is 200 μm. For each treatment group six mice (3 male and 3 female) were used.